World Academy of Science, Engineering and Technology
International Journal of Mechanical and Mechatronics Engineering
Vol:5, No:11, 2011

Multiple-Points Fault Signature's Dynamics Modeling for Bearing Defect Frequencies

Muhammad F. Yaqub, Iqbal Gondal, Joarder Kamruzzaman

***Abstract*—**Occurrence of a multiple-points fault in machine operations could result in exhibiting complex fault signatures, which could result in lowering fault diagnosis accuracy. In this study, a multiple-points defect model (MPDM) is proposed which can simulate fault signature's dynamics for n-points bearing faults. Furthermore, this study identifies that in case of multiple-points fault in the rotary machine, the location of the dominant component of defect frequency shifts depending upon the relative location of the fault points which could mislead the fault diagnostic model to inaccurate detections. Analytical and experimental results are presented to characterize and validate the variation in the dominant component of defect frequency. Based on envelop detection analysis, a modification is recommended in the existing fault diagnostic models to consider the multiples of defect frequency rather than only considering the frequency spectrum at the defect frequency in order to incorporate the impact of multiple points fault.

***Keywords*—**Envelop detection, Machine defect frequency, Multiple faults; Machine health monitoring

I. Introduction

MACHINE health monitoring (MHM) is crucial in all industrial processes to achieve high reliability, reduced man power and scheduled maintenance. Rotary machinery is the crucial component in almost all the industrial processes. In case of rotary machinery, malfunctioning in the operation of the bearing is the most common fault. It has been investigated that 40% of the total machine faults are because of bearing faults [1]. In the bearing faults, certain vibration patterns are generated whenever the rolling element passes the defect position. These vibration patterns vary according to the variations in the machine dynamics. The vibration characteristics frequencies generated by inner race, ball and outer race faults are given in (1)-(3) which are dependent upon speed of rotation and geometry of the bearing [2].

$$f_{ID} = \frac{n}{2} f_{rm}\left(1 + \frac{d_{ball}}{d_{pitch}} cos\phi\right), \quad (1)$$

$$f_{OD} = \frac{n}{2} f_{rm}\left(1 - \frac{d_{ball}}{d_{pitch}} cos\phi\right), \quad (2)$$

M. F. Yaqub is with Monash University, Australia, on study leave from Department of Electrical Engineering, University of Engineering and Technology, Lahore. (Phone: +61-3-512-26568; e-mail: farrukh.yaqub@ monash .edu).

I. Gondal is with Gippsland School of Information Technology, Monash University, Australia. (e-mail: iqbal.gondal@monash.edu).

J. Kamruzzaman is with Gippsland School of Information Technology, Monash University, Australia. (e-mail: joarder.kamruzzaman@monash. edu).

$$f_{BD} = \frac{d_{pich}}{2d_{ball}} f_{rm}\left(1 - \left(\frac{d_{ball}}{d_{pitch}}\right)^2 cos^2\phi\right), \quad (3)$$

where f_{rm}, d_{pitch}, d_{ball}, n and ϕ represent rotational speed, pitch diameter, ball diameter, number of balls and the contact angle as highlighted in Fig. 1.

In MHM, there are many techniques which deal with diagnosis and prognosis of single point machine faults [3-5] and also proposed by the authors [6-10]. Only a few of the techniques deal with multiple point defects [11-13] but this techniques are only limited to the conditions when faults belong to different types (inner-race, outer-race and rolling-element). The existing literature lacks in the study of multiple-points defect when type of the fault remains same but the number of fault points is more than one, such as multiple-points defect on the inner-race, outer-race or rolling-element of the bearing. This study develops a novel model to study multiple-points defects and characterizes their impact in case of existing fault diagnostic and prognostic techniques.

Among different type of bearing faults, such as inner-race, rolling-element or outer-race faults, inner race faults are the most complicated type of bearing faults [5]. In inner race faults, the vibration amplitudes produced by the fault vary with the variation in the position of the defect because of non-uniform radial load distribution as shown in Fig. 1 [5]. The vibration amplitudes strength is higher when fault is in the load zone as compared to the instance, when it is outside the load zone. Moreover, the vibration signatures captured in case of inner-race faults are very weak because accelerometers are mounted at the external periphery of the bearing. This study develops the model for multiple-points defect in the inner race

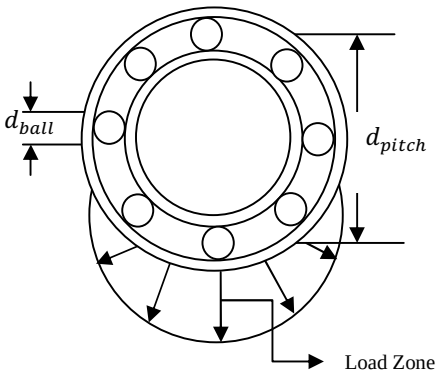

Fig. 1 Rolling element ball bearing geometry.

of the bearing, though extendable to other types of faults as well. The rolling elements in the bearing pass all the points on the inner race of the bearing with the frequency defined in (3). In case of multiple points defect on the inner race of the bearing, the vibrations pattern generated by the contact of rolling elements with one of the fault-point will be the advanced or delayed version of the vibrations generated by the other faults. Based on this observation, this study develops a multiple-points defect model (MPDM) for inner-race fault by extending the single point model proposed in [5]. MPDM contains generalized analytical expressions and has the tendency to simulate fault signatures for n-points fault based on the relative fault locations. MPDM is not only limited to inner-race faults, it may be extended to outer race and ball faults. The second contribution of this study is to identify that the dominant component of defect frequency, which is determined using Hilbert's transform [14, 15], varies in case of multiple-points defect, based on the relative positioning of the fault points. Analytical expressions are derived to validate this variation in the defect frequency. This variation in the location of the dominant defect frequency could mislead the diagnostic and prognostic techniques which are based on the localization of the fundamental component of defect frequency. It is further explored that the dominant component of defect frequency can be shifted to multiples of fundamental defect frequency. In order to diagnose the faults in case of multiple-points defect, it is recommended to consider the multiples of defect frequency rather than only considering the frequency spectrum at the defect frequency.

The paper is organized as follows; Section II presents the proposed multiple-points defect model with the extension of already discussed single point defect model. Moreover, analytical expressions are derived to validate the defect frequency variation and a criterion is proposed to characterize this variation. Section III illustrates results in order to validate the variation in the location of the defect frequency and Section IV presents the concluding remarks.

II. Multiple-Points Defect Model

This section presents the multiple-points defect model in detail. Starting with single point defect, the model is extended to 'n-points' defect. The end result for 'n-points' defect frequency is non-trivial and a criterion is proposed to study the variation in the defect frequency.

A. Single Point Defect

The vibration patterns generated by single point defects [5] can be represented by (4):

$$v(t) = \{(\omega(t) * h_{MR}(t))e^{-\zeta t}\} * \{\sum_{k=-\infty}^{\infty} \delta(t - kT_{IR}) \times \sum_{l=-\infty}^{\infty} h_{LZ}(t) * \delta(t - lT_S)\}. \quad (4)$$

In (4), $\omega(t)$ represents the white noise which incorporates the randomness in the vibration signal. The machine transfer function $h_{MR}(t)$ is a band pass filter which corresponds to the resonant frequency band, and maximum vibration signal strength lies in this frequency band [16]. The convolution, $\omega(t) * h_{MR}(t)$ gives vibrations induced by every impulse generated by the fault point. $e^{-\zeta t}$ represents the exponential decay in the vibration produced by the fault governed by the machine damping factor, ζ. In (4), $(\omega(t) * h_{MR}(t))e^{-\zeta t}$ is the overall impulse response of the machine. Whenever the rolling element passes the defect point, impulse forces are generated. In case of inner-race defect, the defect frequency defined in (1) is the frequency at which rolling-element passes the defect position. So, $T_{IR} = 1/f_{IR}$ is the time period between two consecutive impulses. If the effect of variation in the impulse amplitude is ignored with respect to load zone, the overall vibrations can be given as in (5):

$$v(t) = \{\omega(t) * h_{MR}(t)e^{-\zeta t}\} * \{\sum_{k=-\infty}^{\infty} \delta(t - kT_{IR})\}. \quad (5)$$

In (5), the impact of variation in amplitudes of impulse forces due to load zone is ignored. In case of inner-race fault, the amplitude of impulse forces varies with the position of the defect point. It is due to the repetitive movement of the defect point inside and outside the load zone as provided in Fig. 1. But since the amplitudes of the impulses vary with respect to the load zone, the factor $\sum_{l=-\infty}^{\infty} h_{LZ}(t) * \delta(t - kT_S)$ in (6) incorporates the impact of load zone. $h_{LZ}(t)$ is the component which is responsible for the variation in the impulse amplitudes and is assumed to be the hamming window [5]. As the impact of load zone repeats after every revolution, T_S represents the time per revolution.

$$v(t) = \{\omega(t) * h_{MR}(t)e^{-\zeta t}\} * \{\sum_{k=-\infty}^{\infty} \delta(t - kT_{IR}) \times (\sum_{l=-\infty}^{\infty} h_{LZ}(t) * \delta(t - kT_S))\}. \quad (6)$$

B. Two points defect

Before developing analytical expressions for MPDM, the intuitive understanding is provided. Figure 2 presents a case with two defect positions marked as 'a' and 'b'. Assuming that the inner-race is rotating in the 'anticlockwise' direction, the rolling element 'A' first passes the defect position 'a' and then 'b'. The vibrations produced by defect point 'b' are delayed version of the vibrations produced by defect point 'a'.

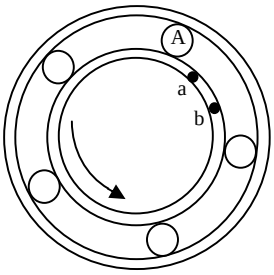

Fig. 2 Two-points defect.

We have seen that the relative locations of the faults are such that the impulses generated by one fault are delayed version of the impulses generated by the other fault. In case of two point faults, the overall vibrations induced by two point fault can be represented as in (7):

$$v''(t) = \{\omega(t) * h_{MR}(t)e^{-\zeta t}\} * \{\sum_{k=-\infty}^{\infty}\delta(t-kT_{IR}) \times \sum_{l=-\infty}^{\infty} h_{LZ}(t) * \delta(t-lT_S) + \sum_{k=-\infty}^{\infty}\delta(t-kT_{IR}-t_d) \times \sum_{l=-\infty}^{\infty} h_{LZ}(t) * \delta(t-lT_S-t_d)\}. \quad (7)$$

In (7), t_d incorporates the time shift (delay) between the impulses generated by two different faults as shown in Fig. 2. In MPDM, it is assumed that the damping factor, ζ is sufficiently large so the pulse smearing is ignorable, i.e., vibrations induced by the impulses of one defect point do not last longer than the time shift between impulses generated by the other defect point. In order to study the variation in the defect frequency, Fourier transform of (7) is derived. Assuming that Fourier transform of $v(t)$ is given by $V(\omega)$, then the Fourier transform of $v''(t)$ is given by (8):

$$|V''(\omega)|^2 = |V(\omega)|^2 \times \{(1+cos\omega t_d)^2 + sin^2\omega t_d\}. \quad (8)$$

Equation (8) is further simplified as in (9). It shows that the vibration frequency spectrum in case of single-point defect is multiplied with a factor of $1+cos\omega t_d$. Based on the value of t_d, this expression has the tendency to hide the fundamental component of defect frequency.

$$|V''(\omega)|^2 = 2 \times |V(\omega)|^2 \times \{1+cos\omega t_d\}. \quad (9)$$

C. Three points defect

Let us assume that the relative locations of the faults are such that the impulses generated by one fault are delayed by t_{d1} and t_{d2} of the impulses generated by the other two faults. The overall vibrations induced by 3-points fault can be represented as in (10):

$$v'''(t) = \{\omega(t) * h_{MR}(t)e^{-\zeta t}\} * \{\sum_{k=-\infty}^{\infty}\delta(t-kT_{IR}) \times \sum_{l=-\infty}^{\infty} h_{LZ}(t) * \delta(t-lT_S) + \sum_{k=-\infty}^{\infty}\delta(t-kT_{IR}-t_{d1}) \times \sum_{l=-\infty}^{\infty} h_{LZ}(t-t_{d1}) * \delta(t-lT_S-t_{d1})\} + \sum_{k=-\infty}^{\infty}\delta(t-kT_{IR}-t_{d2}) \times \sum_{l=-\infty}^{\infty} h_{LZ}(t-t_{d2}) * \delta(t-lT_S-t_{d2})\}. \quad (10)$$

The Fourier transform of $v'''(t)$ is given by (11). In (11), $V(\omega)$ is Fourier transform of the vibration signal in case of single-point defect. It shows that the spectrum of the signal is being multiplied with another factor which determines the variation in the frequency of the vibration signal (detailed results are provided in Section III).

$$\left|V'''^{(\omega)}\right|^2 = |V(\omega)|^2 \times \{(1+cos\omega t_{d1}+cos\omega t_{d2})^2 + (sin\omega t_{d1}+sin\omega t_{d2})^2\}. \quad (11)$$

D. n-points defect

Combining the results in (8) and (11) and assuming that $V(\omega)$ is the frequency response of the vibration signal in case of single-point defect, the Fourier transform of n-point defect can be represented in the generalized notation as in (12):

$$|V^n(\omega)|^2 = |V(\omega)|^2 \times \{(1+\sum_{i=1}^{n-1} cos\omega t_{di})^2 + (\sum_{i=1}^{n-1} sin\omega t_{di})^2\}, \quad (12)$$

or,

$$|V^N(\omega)|^2 = |V(\omega)|^2 \times F_C\left(\omega, t_{d1}, t_{d2}, \dots, t_{d,n-1}\right), \quad (13)$$

$where\ F\left(\omega, t_{d1}, t_{d2}, \dots, t_{d,n-1}\right) = \{(1+\sum_{i=1}^{n-1} cos\omega t_{di})^2 + (\sum_{i=1}^{n-1} sin\omega t_{di})^2\}$.

Equation (13) shows that the Fourier transform of the overall vibration spectrum is being multiplied by another term, i.e., $F\left(\omega, t_{d1}, t_{d2}, \dots, t_{d,n-1}\right)$, we name it as 'defect frequency characterization' function. Throughout the analysis, the defect frequency is determined using envelop detection based on Hilbert's transform [14] as given in (14):

$$v^n(t)_{env} = v^n(t)^2 + [\mathcal{H}\{v^n(t)\}]^2. \quad (14)$$

$\mathcal{H}\{\dots\}$ represents the 'Hilbert' transform of the signal. The Fourier transform of $v^n(t)_{env}$ gives envelop spectrum of the signal.

E. Defect Frequency Characterization Function

$F\left(\omega, t_{d1}, t_{d2}, \dots, t_{d,n-1}\right)$ in (13) characterizes the variation in the defect frequency, and is an n-dimensional function. In case of single point defect, the dominant component of defect frequency lies at $\omega = \omega_o$. In order to find the impact on the defect frequency, i.e., $\omega = \omega_o$, where ω_o corresponds to the fundamental component of defect frequency, we are interested in determining the points of minima. The analytical solution to the problem is very difficult, due to the increased dimensionality as well as it may contain multiple stationary points (as it involves summation of sinusoids) rather than unique global minima (this hypothesis is validated in Fig. 3). A numerical way to solve this function is to use grid search [17]. In grid search, the input-variables, i.e., $t_{d1}, t_{d2}, \dots, t_{d,n-1}$ are varied with a suitable uniform step-size (depends upon the transient behavior of the application) between the extreme limits and the output variable is determined.

Figures 3a-3b present the variation in the characterization function by varying the value of defect point, i.e., t_d. In Figs. 3a-3b, the minimum value of t_d is considered as '0' ('a' and 'b' represent same defect point in Fig. 2) and maximum value as $1/f_{ID}$. Because f_{ID} (1) is defined as the frequency at which the rolling-elements passes the defect point. Figure 3a shows that at $\omega = \omega_o$, by varying the value of t_d, the defect frequency characterization function $F(\omega, t_d)$ changes between maximum and minimum values. The variation in $F(\omega, t_d)$ results variation in the dominant component of defect frequency of the overall vibration signal. Figure 3b plots $F(\omega, t_{d1}, t_{d2})$ for 3-points defect at $\omega = \omega_o$. It shows that by varying the values of t_{di}, $F(\omega, t_{d1}, t_{d2})$ varies.

In Fig. 3a (2-points defect) and Fig. 3b (3-points defect), the characterization function is very simple as in (8) and (9), and stationary points could be determined analytically. In the generalized function, since $F\left(\omega, t_{d1}, t_{d2}, \dots, t_{d,n-1}\right)$ is n-dimensional function, it is very difficult to find the generalized

solution of the equation, so grid search is used. In order to characterize the impact on defect frequency due to multiple-points defect, a criterion is proposed in subsection II-F.

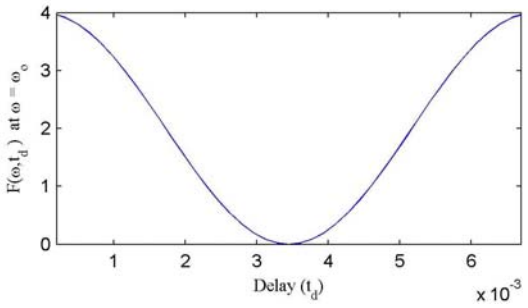

Fig. 3a $F(\omega, t_d)$ *at* $\omega = \omega_o$

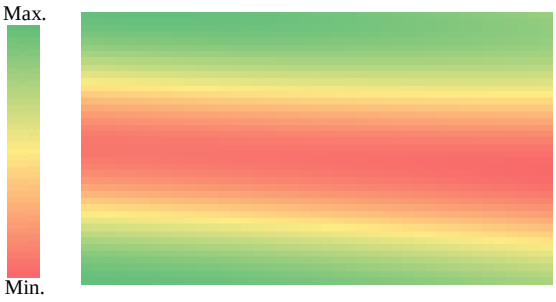

Fig. 3b $F(\omega, t_{d1}, t_{d2})$ *at* $\omega = \omega_o$

F. Dominant Defect Frequency

To determine the impact of multiple-points fault, it is important to define the relation between defect frequency obtained from envelop of the vibration signal and the overall vibration frequency spectrum. Figures 4a-4b present the relationship between the overall vibration frequency spectrum and envelope spectrum. The vibration data is obtained for the single point defect using (4). Figure 4a presents the vibration frequency spectrum of the overall vibration signal [5]. In Fig. 4a, it is clear that the frequency spectrum contains relatively high amplitudes for some of the frequencies. We use the term 'spectral spikes' for these frequencies. Figure 4b plots the envelop frequency spectrum obtained from the Hilbert's transform. It shows that the dominant defect frequency as determined in envelop of the signal (13) (Fig. 4b) is the frequency difference between spectral spikes in the overall vibration signal (Fig. 4a).

In Fig. 4, it shows that the defect frequency is equal to the difference of the spectral spikes in the overall vibration signal. Since, it is not possible to find the closed form solution of (13) due to the curse of dimensionality, the impact of multiple points fault is determined based upon the difference between the spectral spikes in the overall vibration signal. In (15), the procedure is defined to determine the impact of multiple defects at the defect frequencies based upon (13).

$$\{t_{d1}, t_{d2}, \dots, t_{dn}\}_{mf_d} = min\,\{V(\omega, t_{d1}, t_{d2}, \dots, t_{dn}),$$
$$\forall\, \omega = xf_d \wedge rem(x, m) \neq 0. \qquad (15)$$

It is verified using grid search that the dominant component of defect frequency is not always located at the defect frequency but shifts to the multiples of the defect frequency depending upon the relative location of the faults. Intuitively, in order to find the values of t_{di} such that the dominant component of defect frequency is changed as mf_d (integer multiple of the dominant defect frequency in single point fault), the frequency difference between the spectral spikes should be mf_d as in (15), where x is an integer. It is validated in Section III that the minimization problem in (15) developed on the basis of intuitive understanding of the problem, accurately determines the values of t_{di}.

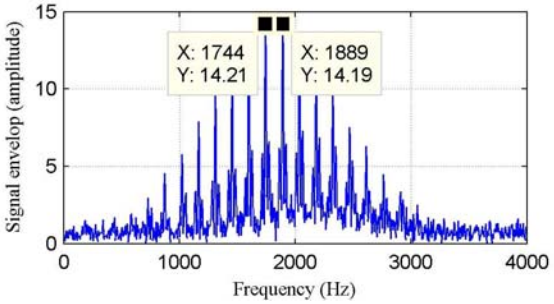

Fig. 4a Envelop of the signal at $t_d = 0.0173$secs.

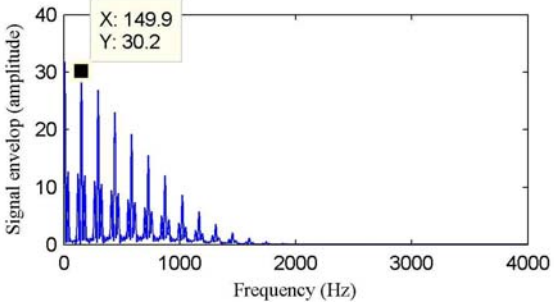

Fig. 4b Envelop of the signal at $t_d = 0.0173$secs.

III. Experimental Results

This section presents results in order to characterize the impact of multiple points fault on the defect frequency. Defect frequency is determined using envelope detection based on Hilbert's transform. The simulated data in these experiments is obtained using Matlab (12). In order to validate the variation in the positioning of the dominant component of defect frequency, only one of the possible scenarios is presented for relative location of the fault points. Results are presented for two points (subsection III-A) and three points defect (subsection III-B), otherwise hold true for n-points defect as well.

A. 2-Points Defect

In order to validate the impact of two points fault on the defect frequency, Figure 5a-c plots the envelop frequency spectrum for three different scenarios. The vibration data is simulated for the 2-points inner-race defect using (7). In Fig. 5a, the frequency spectrum corresponds to the defect

frequency $294.8Hz$ as determined according to the criterion provided in (15). It shows that due to two points defect, the dominant component of defect frequency is changed from $149.9Hz$ (Fig. 4) to $294.8Hz$ (Fig. 5a). Figure 5b shows another scenario in which the dominant component of defect frequency is changed from $149.9Hz$ (Fig. 4) to $439.7Hz$. In Fig. 5c, the dominant defect frequency component lies at $584.6Hz$. The results presented in Fig. 5a-c correspond to the relative positions (delays) of the defect such that $t_d = 0.0034\text{secs}, 0.0022$ and 0.0018secs respectively. In case of two points defects, maximum dominant defect frequency reaches $584.6Hz$. The relative location of the fault points, ie.., t_d are determined using the criterion presented in Subsection II-F. These results show that by varying the relative position of the fault points, the dominant component of defect frequency varies. Moreover, dominant component of defect frequency always lies at the multiples of defect frequency.

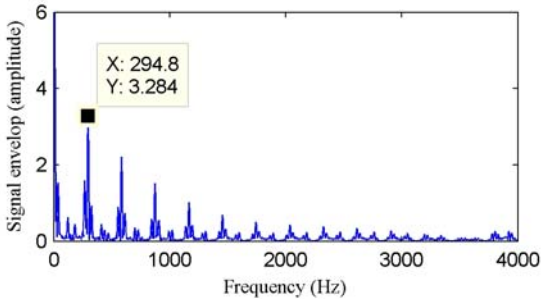

Fig. 5a Envelop of the signal at $t_d = 0.0034\text{secs}$.

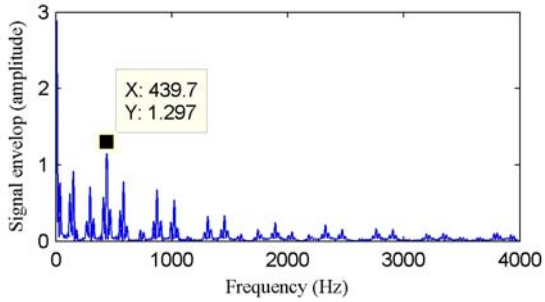

Fig. 5b Envelop of the signal at $t_d = 0.0022\text{secs}$.

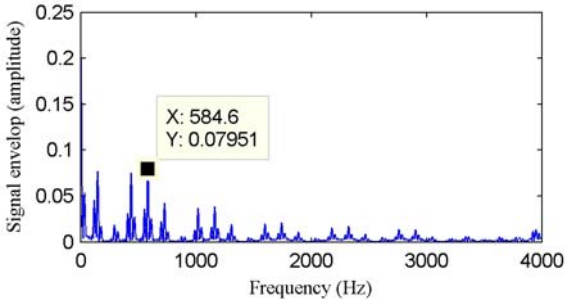

Fig. 5c Envelop of the signal at $t_d = 0.0018\text{secs}$.

B. 3-Points Defect

In case of 3-points faults, it is determined that maximum dominant defect frequency reaches $974.5Hz$. Figures 6a-e plot envelop spectrum of the vibration signal with three points defect with different relative locations of the fault points. In these experiments, the simualted vibration datasets for inner-race fault is obtained using (10). Figures 6a-e correspond to the frequency spectrum of the vibration signal envelop when dominant defect frequencies are $294.8Hz$, $439.7Hz$,

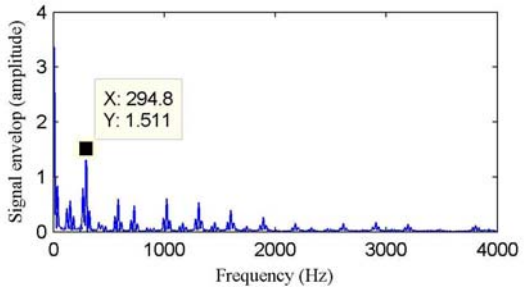

Fig. 6a Envelop of the signal at $t_{d1} = 0.0038$ & $t_{d2} = 0.0007\text{secs}$.

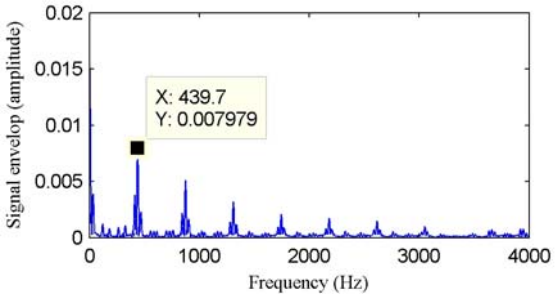

Fig. 6b Envelop of the signal at $t_{d1} = 0.0047$ & $t_{d2} = 0.0023\text{secs}$.

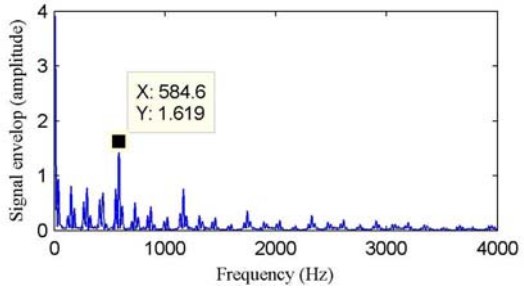

Fig. 6c Envelop of the signal at $t_{d1} = 0.0017$ & $t_{d2} = 0.0052\text{secs}$.

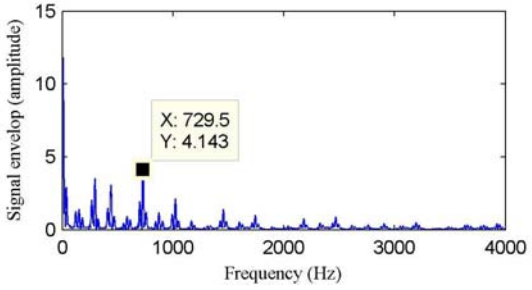

Fig. 6d Envelop of the signal at $t_{d1} = 0.0013$ & $t_{d2} = 0.0042\text{secs}$.

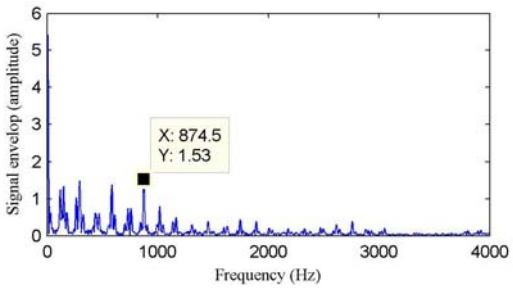

Fig. 6e Envelop of the signal at $t_{d1} = 0.0241$ & $t_{d2} = 0.0080$secs.

$584.6Hz$, $729.5Hz$ and $974.5Hz$ respectively. The relative position of the fault points i.e., t_{d1}, t_{d2} as provided in the Figs. 6a-e, are determined according to the criterion presented in (15) in Subsection II-F. It shows that due to three points defect, the dominant defect frequencies are lying at the multiples of the defect frequency (Fig. 4). Moreover, the comparison with the results presented in subsection III-A for 2-points defect (Fig. 5a-c) shows that the maximum value of the dominant defect frequency increases by increasing the number of defect points.

The results presented in subsections III-A and III-B are only for particular scenarios of the relative defect positions in order to elaborate the impact of multiple points fault. These results validate that that the dominant component of defect frequency is always integer multiple of the actual single point defect frequency. In order to mitigate the impact of multiple points fault, it is vital for the existing fault diagnostic techniques to incorporate the multiples of defect frequency as well but not only the fundamental component of defect frequency.

IV. Conclusion

In this paper, a novel multiple-points defect model is proposed which has the tendency to simulate n-points fault signatures. Moreover, in case of multiple-points fault, the variation in the dominant defect frequency is validated using analytical, intuitive and experimental results. It further signifies that it is vital for the fault diagnostic and prognostic models to incorporate multiples of the defect frequency on contrary to the existing schemes based upon fundamental defect frequency component. The impact of damping factor on the defect frequency is considered as the future works. Moreover, the proposed model is only described for inner-race faults, but its generality holds true for outer-race as well as rolling-elements faults. The findings in MPDM emphasize the need to revise the existing diagnostic and prognostic model in terms of incorporating the variation in dominant defect frequency due to multiple-points faults.

References

[1] J. Morel, "Vibratory monitoring and predictive maintenance," *Techniques de l'Ingénieur, Measurement and Control*, vol. RD, 2002.
[2] M. El Hachemi Benbouzid, "A review of induction motors signature analysis as a medium for faults detection," *IEEE Trans. on Ind. Electron*, vol. 47, pp. 984-993, 2000.
[3] Q. Hu, Z. He, Z. Zhang, and Y. Zi, "Fault diagnosis of rotating machinery based on improved wavelet package transform and SVMs ensemble," *Mechanical Systems and Signal Processing*, vol. 21, pp. 688-705, 2007.
[4] K. Teotrakool, M. J. Devaney, and L. Eren, "Adjustable-Speed Drive Bearing-Fault Detection Via Wavelet Packet Decomposition," *IEEE Trans. on Instrum. and Meas.*, vol. 58, pp. 2747-2754, 2009.
[5] J. R. Stack, T. G. Habetler, and R. G. Harley, "Fault-signature modeling and detection of inner-race bearing faults," *IEEE Trans. on Industry Applications*, vol. 42, pp. 61-68, 2006.
[6] M. F. Yaqub, I. Gondal, and J. Kamruzzaman, "Machine Fault Severity Estimation Based on Adaptive Wavelet Nodes Selection and SVM (Accepted for publication)," in *IEEE International Conference on Mechatronics and Automation*, China, 2011.
[7] M. F. Yaqub, I. Gondal, and J. Kamruzzaman, "Severity Invariant Machine Fault Diagnosis (Accepted for publication)," in *IEEE International Conference on Industrial Electronics and Application*, China, 2011.
[8] M. F. Yaqub, I. Gondal, and J. Kamruzzaman, "Resonant Frequency Band Estimation using Adaptive Wavelet Decomposition Level Selection (Accepted for publication)," in *IEEE International Conference on Mechatronics and Automation*, China, 2011.
[9] M. F. Yaqub, I. Gondal, and J. Kamruzzaman, "Severity Invariant Feature Selection for Machine Health Monitoring," *International Review of Electrical Egnineering*, vol. 6, pp. 238-248, 2011.
[10] M. F. Yaqub, I. Gondal, and J. Kamruzzaman, "Machine Health Monitoring Based on Stationary Wavelet Transform and 4th Order Cumulants (Accepted for publication)," *Australian Journal of Electrical & Electronics Engineering*, 2011.
[11] P. D. McFadden and J. D. Smith, "The vibration produced by multiple point defects in a rolling element bearing," *Journal of Sound and Vibration*, vol. 98, pp. 263-273, 1985.
[12] J. Kleer and B. C. Williams, "Diagnosiing Multiple Faults," *Artificial Intelligence*, vol. 32, pp. 97-130, 1987 1987.
[13] E. Cabal-Yepez, R. Saucedo-Gallaga, A. G. Garcia-Ramirez, A. A. Fernandez-Jaramillo, M. Pena-Anaya, and M. Valtierra-Rodriguez, "FPGA-Based Online Detection of Multiple-Combined Faults through Information Entropy and Neural Networks," *International Conference on Reconfigurable Computing and FPGAs (ReConFig)*, 2010, pp. 244-249.
[14] P. W. Tse, Y. H. Peng, and R. Yam, "Wavelet Analysis and Envelope Detection For Rolling Element Bearing Fault Diagnosis---Their Effectiveness and Flexibilities," *Journal of Vibration and Acoustics*, vol. 123, pp. 303-310, 2001.
[15] R. B. Randall, J. Antoni, and S. Chobsaard, "The relationship between spectral correlation and envelope analysis in the diagnosis of bearing faults and other cyclostationary machine signals," *Mechanical Systems and Signal Processing*, vol. 15, pp. 945-962, 2001.
[16] I. S. Bozchalooi and M. Liang, "A joint resonance frequency estimation and in-band noise reduction method for enhancing the detectability of bearing fault signals," *Mechanical Systems and Signal Processing*, vol. 22, pp. 915-933, 2008.
[17] P. M. Lerman, "Fitting Segmented Regression Models by Grid Search," *Journal of the Royal Statistical Society. Series C (Applied Statistics)*, vol. 29, pp. 77-84, 1980.